24th INTERNATIONAL CONGRESS ON SOUND AND VIBRATION
23–27 July 2017, London

ICSV24
23-27JULY 2017
LONDON CALLING

COMPUTATIONAL INVESTIGATION OF DIRECT NOISE GENERATED BY SYNTHETIC HOT SPOTS IN A DUCT

Jocelino Rodrigues, Erwan O. Rolland, Francesca De Domenico *and* Simone Hochgreb
University of Cambridge, Department of Engineering, Trumpington Street, Cambridge CB2 1PZ, UK
email: jr699@cam.ac.uk

Pressure fluctuations associated with combustion, particularly in gas turbines, are often linked to either the direct gas expansion due to heat release (direct noise) or the passage of temperature or composition non-uniformities through an outlet gas nozzle (indirect noise). Experiments using the Cambridge Entropy Generator (CEG) have been able to separate and measure the contributions between direct and indirect noise in a system with well controlled boundary and operating conditions, suitable for direct comparison with models. The CEG consists of a tube through which air flows at a controlled rate. Temperature variations are generated by Joule heating of a thin wire grid, and are accelerated through an orifice plate operated at sub- or supercritical conditions, with pressure fluctuations measured upstream. Current prediction models assume a 1D propagation of the entropy wave, where the input is the measured temperature. The present work provides a compressible, unsteady RANS simulation for the unsteady temperature and pressure distribution of the CEG experiments, including advection and dispersion of entropy spots. The implementation of the model in OpenFOAM shows that it is possible to capture the behaviour of the experiments, including the evolution of the temperature in time and space, as well as the acoustic signature for different boundary conditions. The model further highlights some of the limitations in representing entropy spots as one-dimensional waves.

Keywords: entropy waves, OpenFOAM, duct, direct noise, hot spots

1. Introduction

Combustion noise has become a major concern within the air and ground based turbine industry. This has been fostered by aircraft design improvements, which allowed for a decrease in other sources of noise, and by the introduction of lean premixed combustion (aimed at reducing nitric oxide emission) which causes more unstable combustion [1]. Of particular interest is not only the propagated noise to the turbine blades, but also the pressure perturbations propagated back into the combustion chamber, which act as a source of combustion instability [2, 3]. The combustion generated pressure perturbations are often classified as direct and indirect noise [4]. Direct combustion noise is generated by the unsteady heat release of a turbulent flame [5]. Indirect combustion noise is caused by the acceleration of entropy spots [6], vorticity waves [7] and/or compositional inhomogeneities [8].

One of the main obstacles in the investigation of entropy noise is the lack of clear data linking entropy and pressure fluctuations, due to complex flame dynamics [9]. Early experiments by Zukoski and Auerbach [10] and Bohn [11] tried to avoid this issue by generating entropy noise using a pulsating heat source through Joule heating of wires. Due to experimental limitations, direct and indirect noise could not be separated. Using this concept, the German Aerospace Centre (DLR) overcame these limitations and developed the Entropy Wave Generator (EWG) rig [12]. The EWG generated

indirect noise, which was captured using microphones downstream of the nozzle. The EWG experiment generated significant interest in the field, leading to numerous attempts at explaining the results numerically [13–16]. Recent work by Becerril *et al.* [17] suggests that the contributions of direct and indirect noise in the subsonic case remain unclear. One of the reasons for this uncertainty is related to the modelling of the acoustic reflections at the inlet and outlet of the rig, which greatly affect the simulated results. More recently, Morgans *et al.* [18] and Giusti *et al.* [19] have taken the first steps in understanding how entropy waves disperse as they advect to the combustor exit.

Entropy Wave Generators similar to the one used at the DLR were developed in Oxford [20] and Cambridge (CEG) [21]. In Cambridge, hot spots were generated with an electric heater and accelerated through an orifice plate, and the noise was measured upstream of the orifice plate. Those results present a clear separation of direct and indirect noise, enabling each to be identified.

The aim of the present paper is to (a) assess the feasibility of using open-source CFD software to model the pressure and temperature in the CEG for comparison with existing experimental data, and (b) to investigate whether assumptions used in one-dimensional thermoacoustic models hold for the CEG. The long term objectives are to develop a tool that can accurately predict direct and indirect noise generation due to synthetic and flame sources.

2. Numerical simulations

2.1 Flow layout and boundary conditions

All computations presented in this paper are related to the CEG experiments by De Domenico *et al.* [21]. The duct has a 42.6 mm inner diameter and was tested using two convective length configurations: short (400 mm) and long (1400 mm). A two-dimensional axisymmetric framework was employed to reduce computational time, taking advantage of the particular geometry. The rotational symmetry was represented by a segment of 2.5 degrees.

Figure 1 (a) shows the geometry used for the open and closed boundary condition test cases. The mesh consisted of 14,800 and 26,350 cells for the short and long configurations, respectively. These were refined near the heating grid and walls to capture the steep temperature gradients and boundary layer effects (Fig. 1 (b)). A uniform velocity profile was used for the inlet, and zero pressure gradient and no-slip velocity boundary conditions were imposed at the walls. A zero gradient pressure condition was imposed at the inlet to simulate an acoustic pressure antinode (and velocity node). For the open tube, a mean atmospheric pressure was enforced at the outlet, as a pressure node and velocity antinode. Walls were assumed to be isothermal (T_0 = 293 K).

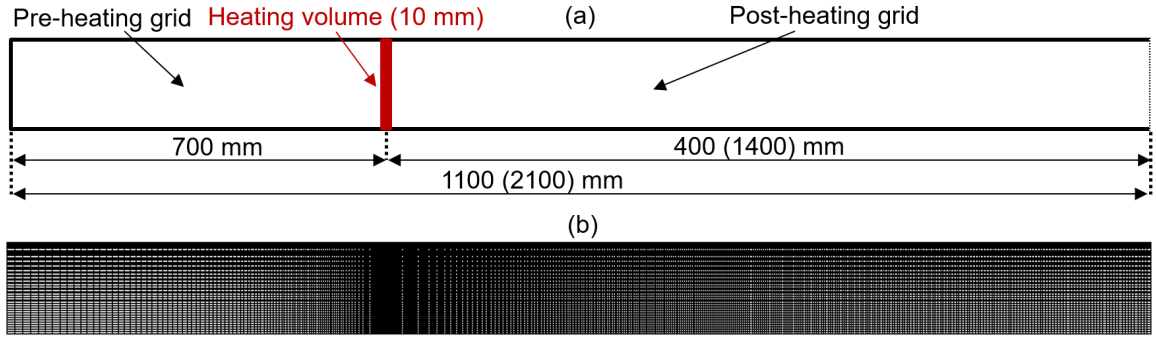

Figure 1: Computational geometry: (a) simplified drawing; (b) mesh (long configuration). Parenthesised values refer to long configuration.

2.2 Numerical setup

The open-source software package OpenFOAM 4.1 was used to perform unsteady, compressible RANS simulations of the steady flow and unsteady heating source in the duct. Momentum and con-

tinuity equations were solved for turbulent compressible flow (Eq. 1), in order to resolve the sound waves.

A volumetric source term, $\dot{S}$, was used to represent the power input by Joule heating across discrete wires, where V is the volume of the modelled computational heating grid.

$$\frac{\partial}{\partial t}\Big[\rho(e+k)\Big] + \nabla\cdot\Big[\rho U(e+k)\Big] + \nabla\cdot(Up) - \alpha_{eff}\Delta(e) = \dot{S} \tag{1}$$

The k-ϵ turbulence model was employed as it showed similar trends to the experimental data (i.e. reduction in centreline temperature with advection through the duct). The numerical study by Mühlbauer et. al. [13] on entropy noise generation in the DLR test rig also employed the k-ϵ turbulence model. The k-ω SST model was investigated, but this showed an increase in temperature at a location where a decrease in temperature was measured in the experiments (at 0.4 m from the grid). The turbulent Prandtl number, Pr_t = 0.7, was used [22, 23]. The inlet turbulent kinetic energy, $k = \frac{3}{2}(UI)^2$, where I is the initial turbulence intensity and a function of the Reynolds number, was set to k = 4.21 x 10^{-3} m^2/s^2 and to k = 0.22 x 10^{-3} m^2/s^2 for U = 0.88 m/s and U = 2.27 m/s respectively.

Probes were positioned in the domain at the same locations where the experimental pressure and temperature fluctuations were measured. For all test cases, a steady-state solution without heat addition was obtained before using sonicFOAM to compute the transient response of the flow to the addition of heat through the source term, $\dot{S}$.

2.3 Modelling of source term, $\dot{S}$

2.3.1 Convected heat input, $\dot{Q}_c$

The source term $\dot{S}$ in Eq. 1 represents the heat transfer per unit volume. This is determined by considering the total electrical power delivered during the heating interval t_p, which is used for heating the wire and the surrounding air:

$$\dot{Q} = m_w c_w \frac{\mathrm{d}T_w}{\mathrm{d}t} + hA_w(T_w - T_\infty) \tag{2}$$

where m_w is is the wire mass, c_w the heat capacity, T_w the wire temperature (assumed to be uniform), A_w the total wire surface area and *h* the convective heat transfer coefficient for flow over a cylinder [24]. T_∞ is assumed to be 293 K. The equation can be solved for T_w where the power to the wires, $\dot{Q}$, starts at time t_0:

$$T_w = T_\infty + \frac{\dot{Q}}{hA_w}\Big(1 - e^{-\frac{(t-t_0)}{\tau}}\Big) \tag{3}$$

where the time constant is determined by:

$$\tau = \frac{m_w c_w}{hA_w} = \frac{\rho_w d_w c_w}{4h} \tag{4}$$

where d_w is the wire diameter. The heat transferred to the air during the pulse can be calculated through:

$$\dot{Q}_c = hA_w(T_w - T_\infty) = \dot{Q}\Big(1 - e^{-\frac{(t-t_0)}{\tau}}\Big) \tag{5}$$

and for times after the heat flow is ceased ($t > t_0 + t_p$):

$$\dot{Q}_c = hA_w\Big((T_{w,max} - T_\infty)e^{-\frac{(t-t_0-t_p)}{\tau}}\Big) \tag{6}$$

so that the source term:

$$\dot{S} = \frac{\dot{Q}_c}{V} \tag{7}$$

where the volume V is approximated as the product of the duct area A and the length of the region for the heating module, L = 10 mm.

2.3.2 *Power pulse, $\dot{Q}$*

The heat convected into the air depends on the profile of the power delivered to the wires, $\dot{Q}$ (Eqs. 5 and 6). $\dot{Q}$ is related to the shape of the current pulse delivered to the heating grid (Fig. 2 (a)). The current was set to its maximum value, i_{max} = 21 A, while the voltage was set to 35 V. This was a good compromise between avoiding frequent wire breakages while still inducing a significant temperature increase to the flow. The heating module has a resistance R $\approx$ 1 Ω, requiring a voltage of $V = iR = 21$ V. For a constant current input, $\dot{Q}_0 = Ri^2$ = 441 W. The excess energy generated is dissipated. However, during the first milliseconds of the pulse, the capacitor in the driving system leads the power supply to release a higher current, before it auto-adjusts the current to its maximum nominal limit. The initial peak in the delivered current (of duration $t_t \approx 0.015$ s) makes the wires warm up faster than they would do with a square pulse.

Preliminary simulations showed that the current surge, although short in duration, is crucial to the correct modelling of the acquired pressure signatures. The additional power supplied to the air during the transient period, t_t, can be modelled by a multiplier factor, α, for the steady state current, i. This factor appears in Fig. 2 (b) as α^2 since $\dot{Q} \propto i^2$. Initially setting α to 3 (since the current during the surge is 3 times larger than at steady-state) yielded results an order of magnitude higher than captured in experiments (ΔT $\sim$200 K). A bulk multiplier factor for the total power, β, was then included to account for the loss of overall power to the copper metal holder during the pulse duration. The final injected energy was estimated to be $\sim$11 J.

Experimental pressure and temperature results from the open tube investigation were used to validate the modelling coefficients for each bulk flow velocity. For all computations, α was set to 1.50; for U = 0.88 m/s and U = 2.27 m/s, β was set to 0.125 and 0.130 respectively. For the closed case, β was set to 0.055. Figure 2 (b) shows the modelled heat input, $\dot{Q}$, and the modelled convected power profile, $\dot{Q}_c$, for the bulk flow velocity, U = 2.27 m/s.

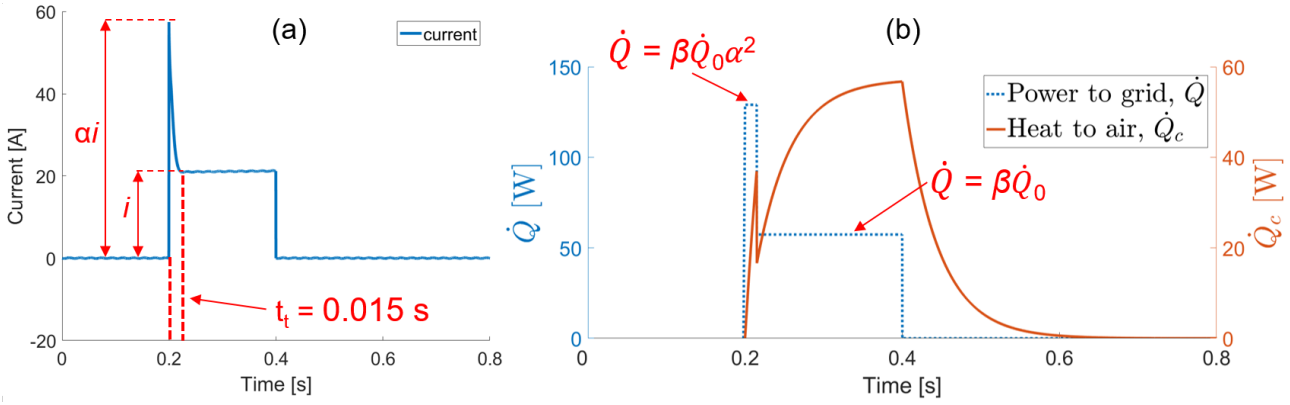

Figure 2: (a) Current delivered to the heating grid driving system;
(b) modelled power input, $\dot{Q}$, and convected power, $\dot{Q}_c$, (α = 1.50, β = 0.130) for U = 2.27 m/s.

3. Results

The response of the system to the generation and convection of synthetic hot spots was measured for two cases: (A) open tube with flow, in which the tube is terminated by an open-end; (B) closed tube with no flow, in which the tube is terminated with a rigid cap. These boundary conditions correspond to two cases considered experimentally, and provide a good benchmark for the feasibility.

3.1 Case A: Open tube

Figure 3 shows pressure signal results for Case A (open-ended tube) with bulk flow velocities U = 0.88 m/s and U = 2.27 m/s, in the long and short tube configurations. The pressure signal measured increases at time zero, in accordance with the expected direct noise from the acceleration

of the flow. Reflections from the open end quickly produce a mode consistent with a quarter wave ($\lambda = L/4$), which is congruous with the imposed boundary conditions of a pressure node at the open end ($R_0 \approx -1$) and a pressure anti-node at the closed end ($R_i \approx 1$). The frequencies calculated from a Fourier transform over 2 s are 79.5 Hz for the short tube and 41.0 Hz for the long tube, in agreement with the theoretical values of 78.0 Hz and 40.8 Hz, respectively, for the same cases. The agreement of experimental and numerical results is encouraging for the long tube. In the case of the short tube, we clearly have resolution and accuracy constraints both in the measurements and calculations for the higher frequency fluctuations, so the agreement is not perfect in intensity. Under ideal conditions of unit reflection coefficient, one would not expect a decay (perfect reflection of either velocity or pressure), yet the experimental and numerical results yield very similar decay rates, arising from the dissipation at the boundaries and through the duct for the long tube. The imperfect calculation of the reflection at the ends leads to a dispersion and dephasing of the waves which is more pronounced in the case of the short tube, for which there are a larger number of reflections per unit time. The intensity of the direct noise p' scales directly with the relative fluctuation in heat release rate q' and Mach number M as $p' = \frac{M}{1-M^2} q'$ [15]. From this, we see that $p' \propto Q_c \propto M^n$ (where n is a function of the Reynolds number). As a result, we expect $\sim$40% increase in direct noise for U = 2.27 m/s when compared to U = 0.88 m/s. This is consistent with the results (Fig. 3).

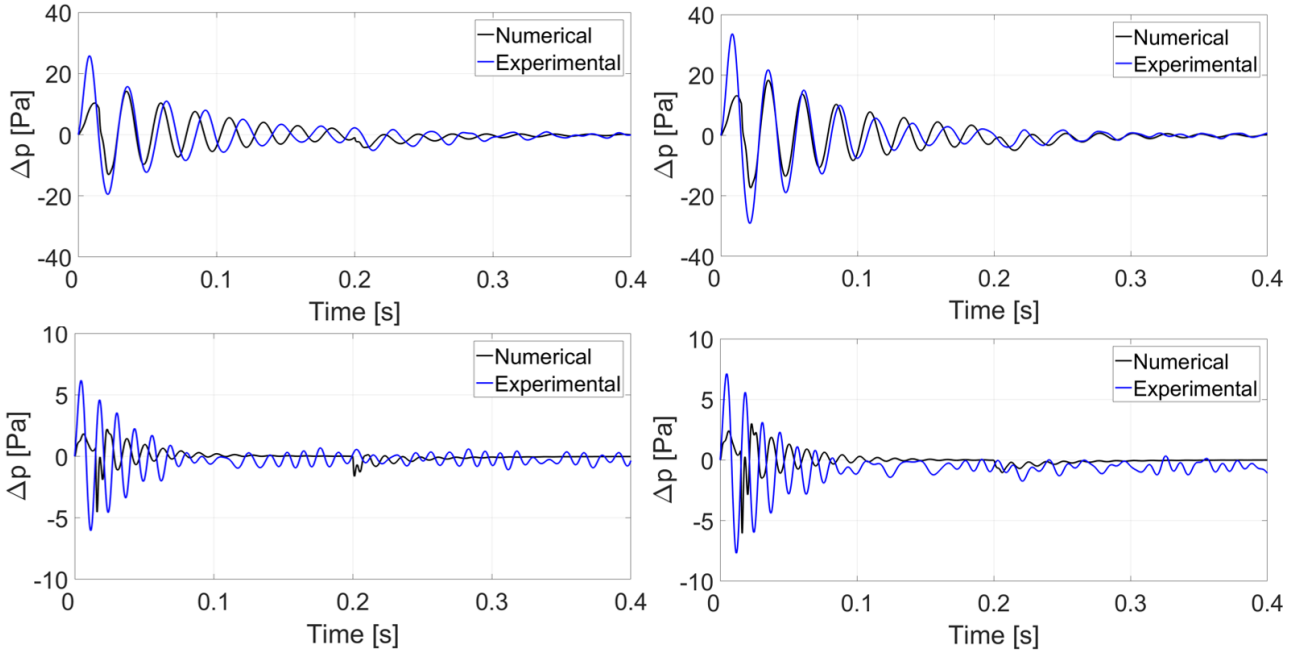

Figure 3: Experimental (averaged) and numerical (single trace) pressure fluctuations for an open-end condition. Left column: U = 0.88 m/s; right column: U = 2.27 m/s. Top: long configuration; bottom: short configuration. Heat addition at t_0 = 0 s.

Figure 4 compares the measured and computed temperatures at different centreline locations. The results agree nicely with a maximum difference of $\sim$0.2 K between the models and the experiments. This is expected, as the power profile was scaled to agree with near-grid measurements. The comparison further downstream shows differences both in the decay and dispersion of the temperature with time. At 0.4 m from the grid, the simulations slightly over-predict the measurements, while at 1.4 m they under-predict. The Reynolds numbers in the duct range from 2481 to 6400, which can prove to be a relatively transitional region where URANS models may not fully capture the dispersion. Further, there could also be differences due to the boundary conditions, where constant temperature may not fully represent the behaviour at the walls.

Figure 5 shows the dispersion of the temperature wave through the long duct at two times during the convection process. The wave clearly disperses axially through the duct from the initial 10 mm (heating module width) to 530 mm (about one quarter of the duct's axial length) towards the end of

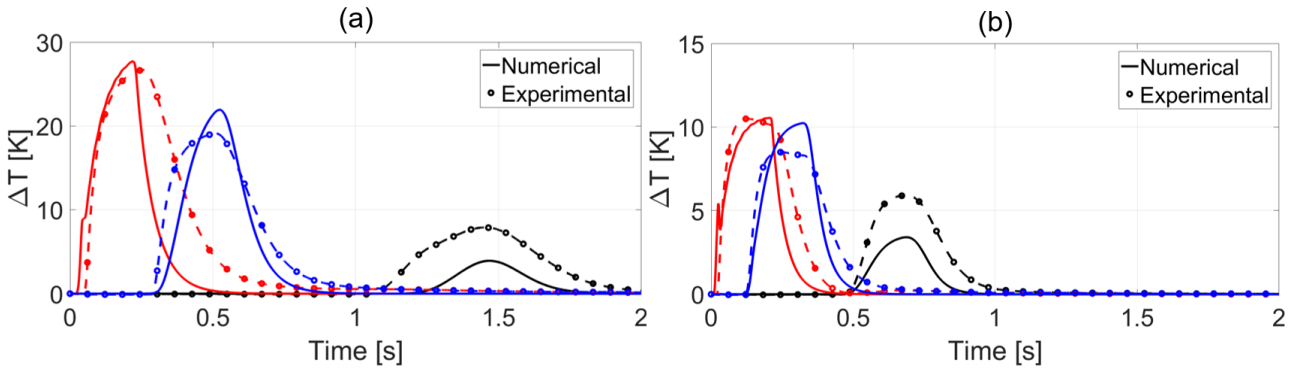

Figure 4: Experimental vs. numerical temperature fluctuations with an open-end condition at 0.04 m from the grid (red), 0.4 m from the grid (blue), and 1.4 m from the grid (black): (a) $U = 0.88$ m/s; (b) $U = 2.27$ m/s. Heat addition at $t_0 = 0$ s.

the pulse ($t = 200$ ms). This changes the local mean temperature, raising questions about the use of perturbation models (which assume a constant mean temperature) to simulate the behavior of entropy spots. Figure 5 (b) shows how the dispersing temperature perturbation advects through the duct once the heating grid is turned off.

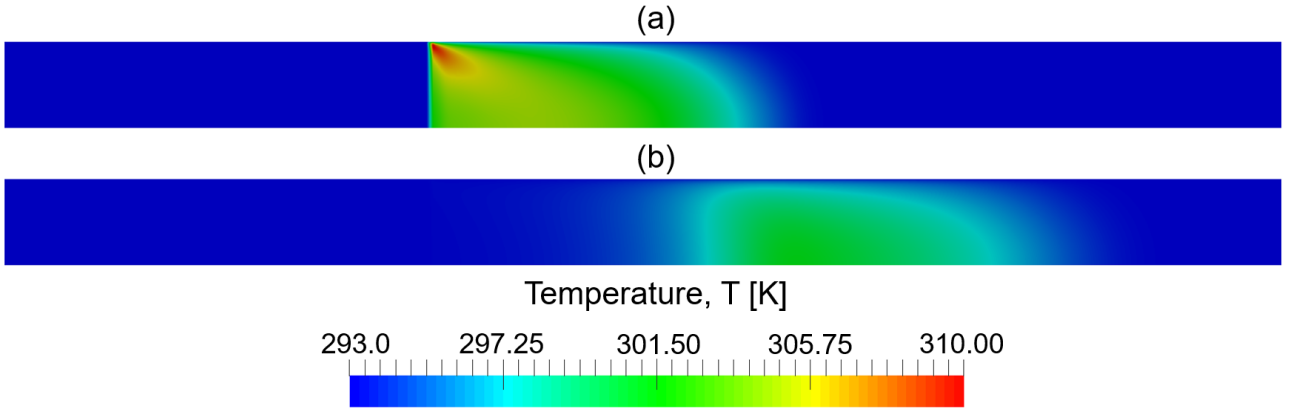

Figure 5: Numerical temperature fluctuations for the long configuration showing the entire domain of 2.1 m, for $U = 2.27$ m/s at different instants after heat addition: (a) $t = 200$ ms (end of pulse); (b) $t = 400$ ms. Figures rescaled by a factor of 0.15 along the axial direction for clarity.

3.2 Case B: Closed tube

Figure 6 shows the results for the closed tube with no mean flow. When the heating grid is activated, the surrounding fluid is heated by conduction and the air expands. This sudden expansion of the fluid, constrained by the inertia of the unperturbed medium, creates a local pressure fluctuation which leads to the generation of acoustic waves which propagate at the speed of sound (thermoacoustic convection) [26]. These waves hit the walls and are reflected back with the same sign as the impinging waves since the boundaries are assumed to be fully reflective ($R_i = R_o = 1$). Given that the acoustic timescale is an order of magnitude smaller than the pulse duration, these acoustic waves add up, or 'reverberate', inside the duct while the heating grid is on. Once the pulse is no longer active, the acoustic energy decays due to viscous and thermal losses within the fluid.

The analytical solution for the heat transfer between grid and air for the zero mean flow condition degenerates, as the value of h depends on conduction and natural convection. Hence, the heat profile for the $U = 0.88$ m/s case was used with a reduced heat input by lowering the value for β (physically explained by the lack of convective heat transfer) to a value of $\beta = 0.055$, for which the pressure growth rate and peak magnitude were accurately captured: for the short tube (blue line) the maximum pressure is higher and the pressure rises faster than for the long tube (black line). This is understandable, since for the short duct, the acoustic round trip time is shorter and thus the acoustic

pressure build up is faster. The very slow decay rates in the pressure compared to the experiment arise because the heat transfer models for stagnant flow are likely not well captured by the current grid: three dimensional gravitational effects are likely to play a role, as are small differences in the reflection coefficient upstream, which is slightly lower than unity in the experiments.

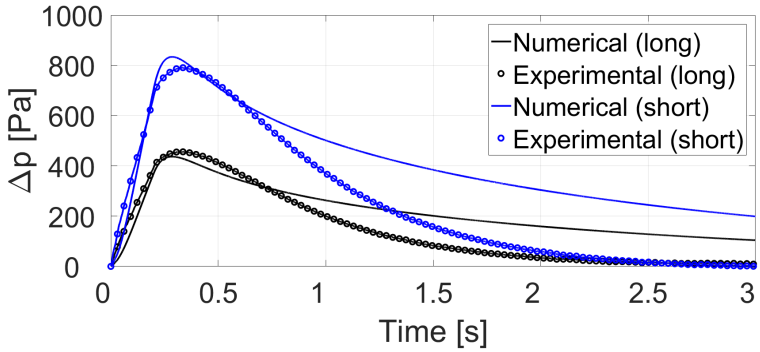

Figure 6: Experimental vs. numerical pressure rise after heat addition with a closed end condition for the short (blue), and long (black) configurations ($\alpha = 1.50$, $\beta = 0.055$).

4. Conclusions

The present preliminary investigations show that OpenFOAM, and specifically sonicFOAM, captures the behaviour of hot spots travelling through a duct, including the acoustic signatures for different boundary conditions and duct lengths. The meshes were found to be appropriately resolved to capture the dispersion of the temperature non-uniformity, as well as the direct noise and its reflections off both ends of the duct. The results showed good agreement with the experimental results, in both the open and closed cases. The spatial non-uniformity seen in the open case temperature results highlights the changes in the mean properties of the flow during the advection of the hot spot. This may need to be taken into account in simplified one-dimensional models.

Further investigations are currently focused on implementing appropriate boundary condition to more accurately model the heat lost to surroundings, as well as capturing the acceleration of hot spots through nozzles and orifices.

Acknowledgements

Jocelino Rodrigues is supported by a Qualcomm/DTA Studentship (University of Cambridge) and Rolls-Royce Plc. Francesca De Domenico is supported by the Honorary Vice-Chancellor's Award and a Qualcomm/DTA Studentship (University of Cambridge). Erwan O. Rolland is supported by an EPSRC DTA studentship (University of Cambridge). Jocelino Rodrigues gratefully acknowledges Dr. Andrea Giusti for his valuable help.

REFERENCES

1. Dowling, A.P. and Stow, S. Acoustic analysis of gas turbine combustors, *Journal of Propulsion and Power*, **19**, 5 (2003), pp. 1–48.

2. Goh, C.S. and Morgans, A.S. The influence of entropy waves on the thermoacoustic stability of a model combustor, *Combustion Science and Technology*, **185**, (2013), pp. 249–268.

3. Polifke, W., Paschereit, C. O. and Klaus, D. Constructive and Destructive Interference of Acoustic and Entropy Waves in a Premixed Combustor with a Choked Exit, *International Journal of Acoustics and Vibration*, **6**, 3 (2001), pp. 135–146.

4. Strahle, W. C. On combustion generated noise, *Journal of Fluid Mechanics*, **49**, 2 (1971), pp. 399–414.

5. Bragg, S. L. Combustion Noise, *Journal of the Institute of Fuel*, **36**, 264 (1963), pp. 12–16.

6. Marble, F. E. and Candel, S.M. Acoustic disturbance from gas non-uniformities convected through a nozzle, *Journal of Sound and Vibration*, **55**, 2 (1977), pp. 225–243.

7. Kings, N. and Bake, F. Indirect combustion noise: noise generation by accelerated vorticity in a nozzle flow, *International Journal of Spray and Combustion Dynamics*, **2**, (2010), pp. 253–266.

8. Magri, L., O'Brien, J. and Ihme, M. Compositional inhomogeneities as a source of indirect combustion noise, *Journal of Fluid Mechanics*, **799**, 4 (2016), pp. 1–12.

9. Dowling, A.P. and Mahmoudi, Y. Combustion noise, *Proc. Combust. Inst.*, **35**, 1 (2015), pp. 65–100.

10. Zukoski, E. E. and Auerbach, J. M. Experiments Concerning the Response of Supersonic Nozzles to Fluctuating Inlet Conditions, *Journal of Engineering for Power*, **98**, 1 (1976).

11. Bohn, M. S. Noise produced by the interaction of acoustic waves and entropy waves with high-speed nozzle flows. PhD thesis, California Institute of Technology (1976).

12. Bake, F., Richter, C., Mühlbauer, B., Kings, N., Röhle, I., Thiele, F. and Noll, B. The Entropy Wave Generator (EWG): A reference case on entropy noise, *Journal of Sound and Vibration*, **326**, 3-5 (2009).

13. Mühlbauer, B., Noll, B. and Aigner, M. Numerical Investigation of the Fundamental Mechanism for Entropy Noise Generation in Aero-Engines, *Acta Acustica United with Acustica*, **95**, (2009), pp. 470–478.

14. Leyko, M., Nicoud, F. and Poinsot, T. Comparison of Direct and Indirect Combustion Noise Mechanisms in a Model Combustor, *AIAA Journal*, **47**, 11 (2009), pp. 2709–2716.

15. Duran, I., Moreau, S. and Poinsot, T. Analytical and Numerical Study of Combustion Noise Through a Subsonic Nozzle, *AIAA Journal*, **51**, 1 (2013), pp. 42–52.

16. Lourier, J., Huber, A., Noll, B. and Aigner, M. Numerical Analysis of Indirect Combustion Noise Generation Within a Subsonic Nozzle, *AIAA Journal*, **52**, 10 (2014), pp. 2114–2126.

17. Becerril, C., Moreau, C., Bauerheim, M., Gicquel, L. and Poinsot, T. Numerical investigation of combustion noise: The Entropy Wave Generator, *22nd AIAA/CEAS Aeroacoustics Conference*, (2016).

18. Morgans, A. S., Goh, C. S. and Dahan, J. A. The dissipation and shear dispersion of entropy waves in combustor thermoacoustics, *Journal of Fluid Mechanics*, **733**, (2013).

19. Giusti, A., Worth, N. A., Mastorakos, E. and Dowling, A. P. Experimental and Numerical Investigation into the Propagation of Entropy Waves, *AIAA Journal*, **55**, 2 (2017), pp. 446–458.

20. Hake, M. I., Experimental Design to Determine the Effect of Temperature and Mach Number on Entropy Noise. PhD thesis. Massachusetts Institute of Technology (2014).

21. De Domenico, F., Rolland, E. O. and Hochgreb, S. Detection of direct and indirect noise generated by synthetic hot spots in a duct, *Journal of Sound and Vibration*, **394**, (2007), pp. 220–236.

22. Malhotra, A. and Kang, S. S. Turbulent Prandtl number in circular pipes, *International Journal of Heat and Mass Transfer*, **27**, (1984) pp. 2158–2161.

23. McEligot, D. M. and Taylor, M. F. The turbulent Prandtl number in the near-wall region for Low-Prandtl-number gas mixtures, *Int. J. Heat Mass Transfer.*, **39**, (1996) pp. 1287–1295.

24. Bergman, T. L., Lavine, A. S., Incropera, F. P. and DeWitt, D. P. Fundamentals of Heat and Mass Transfer, 7th edition, (2011).

25. Munt, R. M. Acoustic Transmission Properties Of A Jet Pipe With Subsonic Jet Flow: I. The Cold Jet Reflection Coefficient, *Journal of Sound and Vibration*, **142**, 3 (1990), pp. 413–436.

26. Trilling, L. On thermally induced sound fields, *J. Acoust. Soc. Am.*, **27**, 3 (1955), pp. 425–431.